Finite Element Simulation of Crack Propagation for α-Ti Based on Cohesive Zone Law Deriving from Molecular Dynamics

Yi Liao[1], Xiangguo Zeng[1], Jun Chen[2], Rongpeng Xu[1,3]*, Huayan Chen[1]

[1] College of Architecture and Environment, Sichuan University, Chengdu, 610065, PR China
[2] Institute of Applied Physics and Computational Mathematics, Beijing, 100094, PR China
[3] School of Engineering, Alfred University, Alfred, NY, USA 14802
Corresponding author: xuyun14567@163.com

Abstract In order to parameterize and obtain a traction-separation (T-S) law, molecular dynamics (MD) simulations via Large-Scale Atomic/Molecular Massively Parallel Simulator (LAMMPS) are used at atomic scale for the deformation and fracture for models with dimension of 200Å×204Å×8.82Å with crack for alpha titanium (α-Ti) with HCP crystal structure under tensile loadings at different loading directions. Visualization of the atomistic configurations during deformation is realized by use of ATOMEYE. It can be concluded that crack extension are correlate with the α-Ti crystal structure and crystal orientation intrinsically. We also found that HCP→BCC phase transition and twin deformation occur in the vicinity of the crack tip for HCP α-Ti under different loading directions via the common neighbor analysis (CNA). The complex mechanisms of deformation, i.e., phase transition, twin deformation, and failure, i.e., crack blunting and extension, were contained in the traction-separation (T-S) law. Then, the generated parameterized traction-separation law is implemented in the finite element model with the behavior of the CZM governed by traction-separation (T-S) law. Finally, the ABAQUS finite element commercial software is employed to simulate the crack propagation behavior for α-Ti CT specimen.

Keywords Alpha Titanium, Molecular dynamics, Cohesive zone model, Crack propagation, Finite element

1. Introduction

Titanium has two kinds of superior properties: high specific strength and corrosion resistant. Titanium has long had appeal to metal designers and material scientists[1]. Commercially, pure titanium is, of course, alpha titanium (α-Ti). Its elemental crystal structure is closed-packed hexagonal, as illustrated in Fig.1[2]. Alpha titanium is anisotropic material. The mechanical properties in its different crystal orientations have significant difference. In this paper, the micro-deformed mechanisms of α-Ti on different conditions of loading are obtained by means of open source MD code LAMMPS[3] developed by Sandia. Visualization of the atomistic configurations during deformation is realized via ATOMEYE software[4].

Xu and Needleman[5,6] first related the cohesive zone model (CZM) with finite element analysis, and they successfully applied it to simulate crack propagation problems. Cohesive elements that possess zero volume in an undeformed state are inserted between bulk elements. They are particularly appropriate when the crack propagation path can be determined. Cohesive zone law defines the relation between traction and crack opening displacement. Because it is difficult to direct experimentally quantify the relation, construction of such a law has been a challenging task in the past decade[7,8]. The traction-separation (T-S) relationship in a CZM is generally parameterized through empirical data.

Our approach to studying crack propagation has included the use of MD simulation for obtaining the functional form of parameterized T-S relations in cohesive elements[9,10]. This paper simulated a compact tension fracture mechanics specimen through cohesive elements whose T-S relation was derived from MD simulations. These results enable us to make several recommendations to improve the methodology to obtain cohesive laws and better comprehend the crack propagation behavior of

α-Ti.

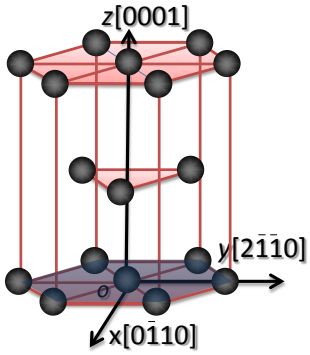

Figure 1. The elemental crystal structure of α-Ti

2 EAM/alloy potential function

Zhou[11]have developed a procedure to generalize the conventional EAM potentials and their cut-off distance. These potentials are well fitted to basic material properties such as lattice constants, elastic constants, modulus of bulk.

In the generalized EAM (EAM/alloy) potential, the total energy E of the crystal can be expressed as:

$$E = \frac{1}{2}\sum_{i,j,i\neq j}\phi_{ij}\left(r_{ij}\right) + \sum_{i}F_i\left(\rho_i\right) \tag{1}$$

Where ϕ_{ij} represents the pair energy between atoms i and j separated by r_{ij}, and F_i stands for the embedding energy to embed an atom i into a local site with electron density ρ_i. ρ_i can be calculated using:

$$\rho_i = \sum_{j,j\neq i} f_j\left(r_{ij}\right) \tag{2}$$

With $f_j(r_{ij})$ the electron density at the site of atom i arising from atom j at a distance r_{ij} away. Alloy EAM potentials can be constructed from elemental EAM potentials if the potentials are normalized and unified cutoff functions are used. To fit such an EAM potential set, the generalized pair potentials were chosen to have the form:

$$\phi(r) = \frac{A\exp\left[-\alpha\left(\frac{r}{r_e}-1\right)\right]}{1+\left(\frac{r}{r_e}-\kappa\right)} - \frac{B\exp\left(-\beta\left(\frac{r}{r_e}-1\right)\right)}{1+\left(\frac{r}{r_e}-\mu\right)^{20}} \tag{3}$$

Where r_e is the equilibrium spacing between nearest neighbors, A, B, α, β are four adjustable parameters, andκ , μ are two additional parameters for the cut off[12].

The electron density function is taken with the same form as the attractive term in the pair potential with the same values of β, and μ, i.e.,

$$f(r) = \frac{f_e\exp\left[-\beta\left(\frac{r}{r_e}-1\right)\right]}{1+\left(\frac{r}{r_e}-\mu\right)^{20}} \tag{4}$$

Table1. EAM potential parameters of titanium

R_e(Å)	f_e	ρ_e	α	β	A	B	μ	κ
2.933872	1.863200	25.56513	8.775431	4.680230	0.373601	0.570968	1.0	0.5

The potential function usually is empirical, and it is also controversial in MD simulation. The melting point of α-Ti was obtained by LAMMPS in order to verify the EAM/alloy potential. The atomic structure of α-Ti is shown in Fig.1. The initial configuration of the simulated system was composed of 8×8×5 HCP-Ti cellular, a total of 1280 atoms, the time step was 0.01*ps*, using three-dimensional periodic boundary conditions, let the system in the 2.5*K* relaxation 500000 steps, and then use the Nose-Hover method to keep the pressure around zero, and then elevated system temperature from T=2.5*K* to 2500*K*. During the simulation, the thermodynamic results were output every 1000 steps, as shown in Fig.2 and Fig.3 respectively. The average atomic volume almost linear increases with the temperature and simulation time in the heating process. But it suddenly jumps when the temperature reaches a certain value. This phenomenon indicated that the system had undergone some kind of phase transition. The melting point of α- T_i is about 1951*K*, and simulation value is 1943*K* near a phase transition. The error between them is about 0.41%. Such deviation derived from the melting point between the MD simulation and the actual sample were relatively consistent, which was related with using three-dimensional periodic boundary conditions in simulation system, the limited number of particles and the accuracy of interaction potential.
The EAM/alloy potential function parameters, which were evaluated by melting point test were shown in Table1.

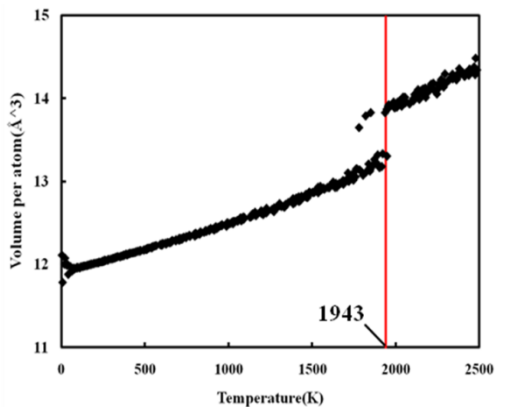

Figure 2. The mean volume of single atom changing with temperature during heating process.

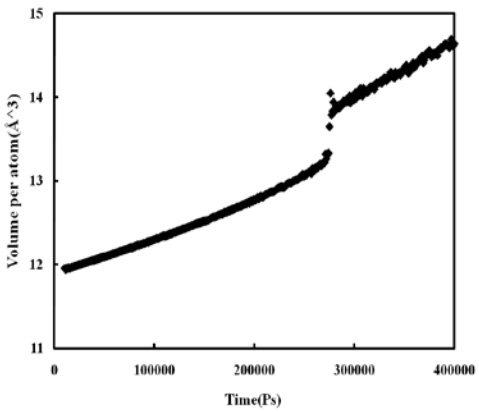

Figure 3. The mean volume of single atom changing with modeling time during heating process.

3 Specimen setup

Due to anisotropic characteristic of α-Ti, it is very meaningful for comprehending failure mechanism of material on different conditions of loading.
The MD models with different loading directions used for conducting fracture studies were shown in Fig.4 and 5. The MD model in Fig.4 showed that the loading direction was $[0\bar{1}10]$, while it was $[0001]$ in Fig.5. The dimensions in the x-y plane are $200Å \times 204Å$ with thickness in the z-direction

equaling 9.64*Å*. The length of crack is 70*Å* in the two models. Non-periodic and shrink-wrapped boundary conditions were used in the x and y directions, while it was periodic boundary in the z-direction. Before loading, the whole system was made relax freely till the valley of energy status. During MD simulations of tensile crack propagation, the boundaries were stretched by moving different distance increment on different regions of boundaries in the Y-direction at each time step. Molecular dynamics simulation time step was given with t=0.005*ps*.

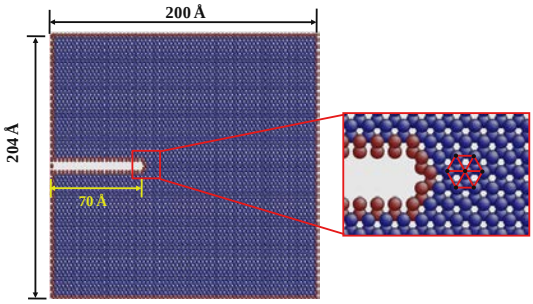

Figure 4. MD model with loading direction $[0\bar{1}10]$

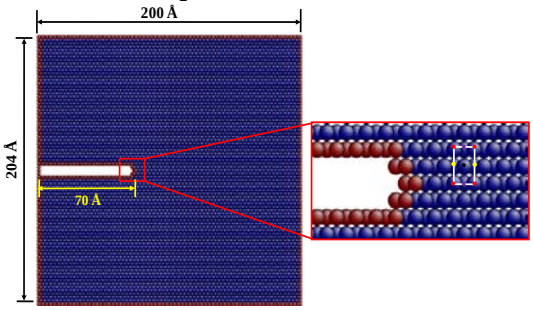

Figure 5. MD model with loading direction [0001]

For the loading condition shown in Fig.4, the phenomenon observed in model by means of CNA was shown in Fig.6. Step=0 indicated that the relaxation was finished. The energy of the system reached minimal. With the increment of loading, crack constantly opened. When the loading increased to Step=3600，it was obvious that crack tip successively emitted dislocations along crystal orientation $[2\bar{1}\bar{1}0]$ and $[\bar{2}110]$ respectively[13]. The phenomenon continued in the whole process of loading. With the emission of dislocation, crack tip moved forward slowly and the crack blunting phenomenon is obvious at crack tip. When Step=8400, we also found that HCP→BCC phase transformation in the vicinity of the crack tip for α-Ti via CNA. The values of CNA corresponding to different atomic structure were displayed in Fig.6.

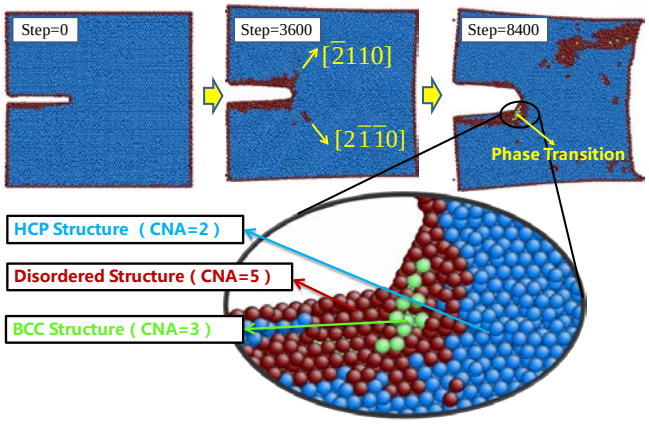

Figure 6. Deformed mechanisms of α-Ti on the condition of loading direction $[0\bar{1}10]$

When Step=2200, there was region where atoms arranged disorderedly near the crack tip. With the increment of loading, the deformed region expanded in the vicinity of the crack tip. When Step=3000, it was obvious that some red atoms (CNA=5) surrounded a lump of blue atoms (CNA=2) in Fig.7. The structure of atoms is identical in the inside and outside of the region that the

red atoms surrounded, but their orientations were different. The orientations of lattice deflected to form twin deformation. The area of twin band increased following the crack propagation. From the crack propagation deformation in Fig.6 and Fig.7, it was shown that twin crystal easily occurred for α-Ti under loading direction $[0001]$, while phase transition and dislocation easily happened under loading direction $[0\bar{1}10]$. Dislocation and twin are two kinds of principal mechanisms for α-Ti.

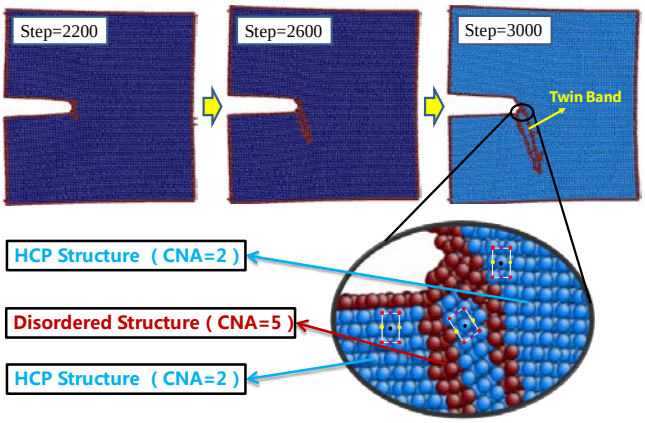

Figure 7. Deformed mechanisms of α-Ti on the condition of loading direction $[0001]$

4 Traction-separation response

To quantify the cohesive zone law, stresses and displacements at local positions are analyzed in detail. MD simulation is conducted for loading direction $[0\bar{1}10]$ at temperature of $300K$ to develop traction-separation relationships for the CZM.

Tensile (σ_{yy}) traction is calculated as the average atomic stress at a distance of ± 20 Å adjacent to the crack. The region is called T-S region, as illustrated in Fig.8. As this stress is calculated locally near the crack surface it therefore relates to the traction in the traction-separation law[8,9,13,14]. The crack opening displacement (separation) was also calculated from the average displacement of the atoms in T-S region. The opening displacements in normal direction therefore are defined and measured as the average atom displacement in Up Region with respect to Down Region. The average traction and opening displacement associated with region were calculated using all the atoms in T-S region. This effectively reduces the scatter of the data.

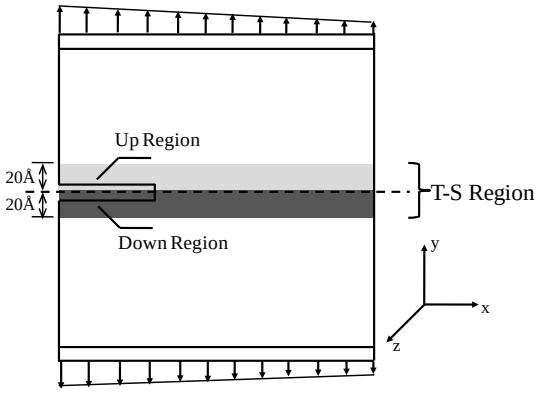

Figure 8. T-S region selected and loading form

The simulation process applying *NVE* system tracking and in every time step, maintain the

temperature of 300*K*, constantly through re-calibration of the speed of atoms. Ladder-shaped loading is applied on the boundary, as shown in Fig.8.

From Fig.9, the traction initially increases as the crack opening distance was increased until they reached a peak value, then decreased as the crack opening was further increased. To represent the CZM, a model that includes an exponential term is suggested to approximate the traction-separation response for tensile mode failure. The complex mechanisms of deformation, i.e., phase transition, dislocation, and crack blunting, were contained in the traction-separation (T-S) law. *A* in the T-S curve indicated damage occurred, which was shown by the typically non-linear decreasing of the curve. It corresponded to remarkable dislocations emission in the crack tip. *B* in the curve corresponds with the moment at which phase transition occurs in the MD model. The curve shows a wide scatter band in the region beyond the elastic deformations, since the data contain traction and separation in all stages of atoms along the crack path. During initial crack growth the scatter band in the cohesive law is very large. This behavior implies that the initial crack starts to grow at different maximum tractions and is not in a steady-state. With crack propagation, the scatter band becomes narrow, which indicates that crack growth becomes steady[15].

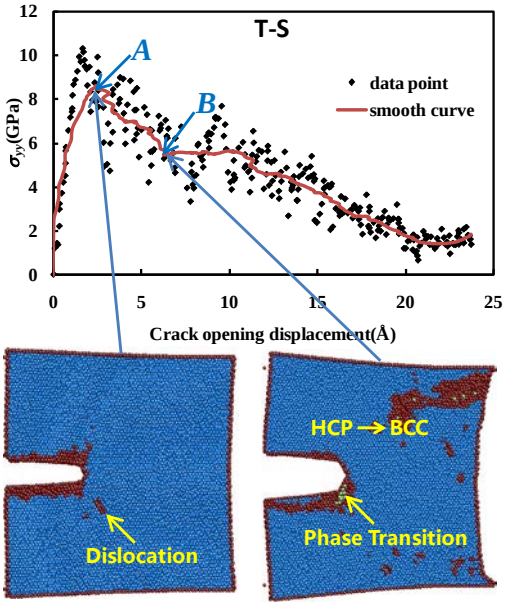

Figure 9. Traction-Separation relationship for α-Ti under tensile loading

A relationship between the traction and the crack opening displacement must be obtained when we use cohesive element. In the CZM, the fracture process zone is simplified as being an initially zero-thickness zone, composed of two coinciding surfaces. Under loading, the two surfaces separate and the traction between them varies in accordance with a specified T-S law. In our study a parameterized exponential T-S law is proposed based on the MD simulations. The traction-separation law ($F(\lambda)$) is then implemented through Eq.(5). The non-dimensional parameter (λ) in Eq. (5) relates the normal (u_n) separation to the maximum allowable normal (δ_n) separation of the cohesive element[14]. In Eq.(5) the maximum cohesive strength (σ_{max}) is simulated at room temperature. The constants in Eq.(5) are obtained in table 2. According to Eq.(5) and table 2, the fitting curve of traction-separation relationship has been illustrated in Fig.10.

$$F(\lambda) = A\sigma_{\max}\lambda^{c}\exp(-B\lambda)(1-0.001T)$$
$$\lambda = u_n / \delta_n \tag{5}$$

Table 2 The constants in Eq.(12)

Simulated temperature (K)	$\sigma_{max}(GPa)$	A	B	C
300	8.61	3.75	2.73	0.37

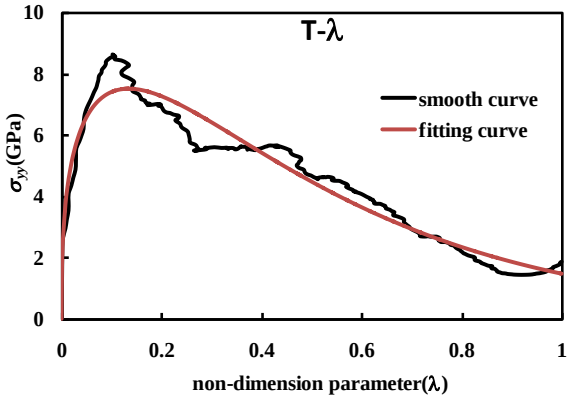

Figure 10. T-λ relationship

5. Simulation of the T-S fracture test

In order to model stable crack growth under static loading and analyze cohesive behavior derived from MD towards greater length scales, we perform a simulation of crack growth for a CT specimen subject to displacement loading via prescribed motion of loading pins. Fracture of a CT specimen can verify whether the cohesive law derived from MD simulations displays behavior consistent with linear elastic fracture mechanics. The geometry and mesh of our CT specimen is shown in Fig.11. The specimen is 384 *nm* wide by H = 369 *nm* tall, with an effective width (the distance between the pin holes and the uncracked edge) of W = 307 nm, an initial crack length of a = 155 *nm* ($a/W \approx 0.5$), and pin holes of radius 38.4 *nm*. Cohesive elements are placed along the predefined crack path, and are 1*Å* wide. The displacement loadings are applied on reference points, i.e. PR-1 and PR-2. The parameterized T-S law given was implemented in ABAQUS to simulate the behavior of the CZM.

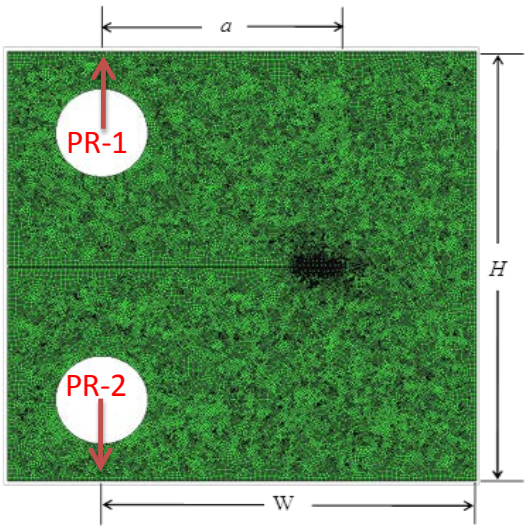

Figure 11. FEA mesh of CT specimen. The specimen's height H =369nm, its effective width W=307nm, and its initial crack length a =155nm

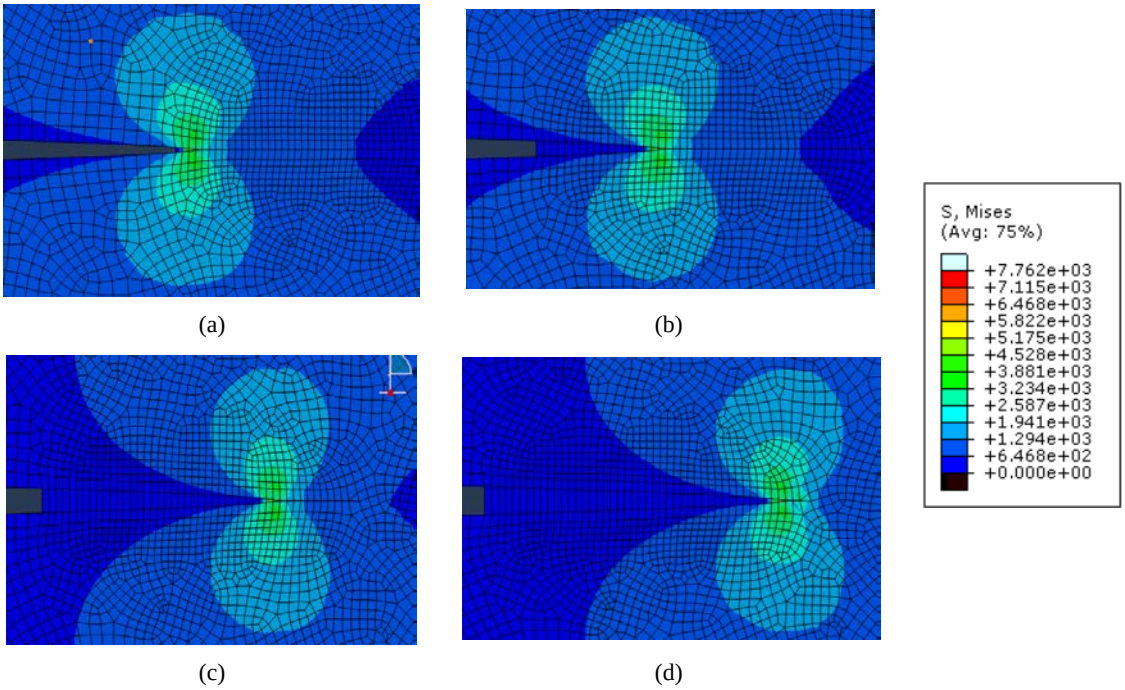

Figure 12. Static crack growth in the CT geometry, plots are colored according to element values of σ_{yy} in units of *GPa* as shown in the legend

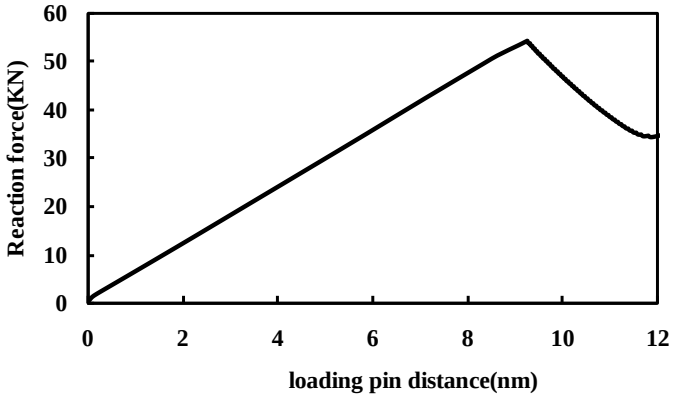

Figure 13. Reaction force versus loading-pin displacement for CT specimen

The crack opening behavior due to displacement of the top and bottom pins is observed in Fig.12. Before crack propagation begins to occur, the cohesive zone begins to form, as shown in Fig.12(a) and (b). Once a critical displacement is reached, crack propagation is seen in Fig.12(c) and (d).
It shows the expected linear relationship between loading-pin displacement and reaction force in Fig.13. More complex fracture mechanics problems can be analyzed through combining the cohesive law derived from MD simulations and finite element method.

6. Conclusion

(1) Molecular dynamics simulations under a special configuration have been performed to study the mechanism of α-Ti under tensile loading condition, and the EAM/alloy potential used in LAMMPS is certified by melting point verification.
(2) Crack tip successively emitted dislocations along crystal orientation $[2\bar{1}\bar{1}0]$ and $[\bar{2}110]$ respectively for loading direction $[0\bar{1}10]$. The phenomenon continued in the whole process of loading. With the emission of dislocation, crack tip moved forward slowly and the crack blunting phenomenon is obvious at crack tip. In the process, we also find that HCP→BCC phase transformation near the crack tip for α-Ti via CNA. It is obvious that twin occurred for α-Ti under loading direction $[0001]$. Dislocation and twin are two kinds of principal mechanisms for α-Ti. The deformation mechanisms of α-Ti are included in the T-S curve derived from MD simulations.
(3) The traction-separation relation of α-Ti with crack is characterized via MD simulations. The parameterized cohesive traction-separation relation under tensile loading condition at room temperature to simulate the crack propagation behavior of *CT* specimen composed of α-Ti in a FEA. The curve obtained through our simulation is agreement with predictions from linear elastic fracture mechanics, showing the expected linear relationship between loading-pin displacement and reaction force. It shows our methodology is feasible. Our study may provide several novel ideas for simulating complex fracture problems based cohesive laws used in FEA.

Acknowledgements

This work was supported by the National Defense Basic Scientific Research Program of China through the contract of B1520132013 and the Fundamental Research Funds for the Central Universities through the contract of 2010SCU21014 and NSAF through the contract of 10776023.

References

[1] J.D.Matthew, Jr. Titanium-A Technical Guide. ASM INTERNATIONAL™ Metal Park, 1988.
[2] C Leyens, M Peters. Titanium and Titanium Alloys. WILEY-VCH GmbH & Co. KGaA. Weinheim, 2003.
[3] S J Plimpton. Fast parallel algorithms for short-range molecular dynamics. J Comput Phys 1995;117:1–19. <http://lammps.sandia.gov/>.
[4] J Li. AtomEye: an efficient atomistic configuration viewer. Modell Simul Mater Sci Eng 11 (2003) 173.

[5] X.P. Xu , A. Needleman, Numerical simulations of fast crack growth in brittle solids, J. Mech. Phys. Solids 42 (1994) 1397-1434.

[6] X.W.Zeng, Shaofan Li, A multiscale cohesive zone model and simulations of fractures. Comput. Methods Appl. Mech. Engrg. 199 (2010) 547–556.

[7] X.W. Zhou, J.A. Zimmerman et al, Molecular dynamics simulation based cohesive surface representation of mixed mode fracture, Mechanics of Materials 40 (2008) 832-845.

[8] X.W. Zhou, N.R. Moody, R.E. Jonesa, J.A. Zimmermana, E.D. Reedyc, Molecular-dynamics-based cohesive zone law for brittle interfacial fracture under mixed loading conditions: Effects of elastic constant mismatch. Acta Materialia, 57 (2009) 4671–4686.

[9] V.Yamakov, E.Saether, D.R.Phillipsc, E.H. Glaessgen. Molecular-dynamics simulation-based cohesive zone representation of intergranular fracture processes in aluminum. Journal of the Mechanics and Physics of Solids. 54 (2006) 1899–1928.

[10] J.T. Lloyd, J.A. Zimmerman, R.E. Jones, X.W. Zhou, D.L. McDowell, Finite element analysis of an atomistically derived cohesive model for brittle fracture. Modelling Simul. Mater. Sci. Eng., 19 (2011) 065007.

[11] X.W. Zhou, H.N.G.Wandley, R.A.Johnson, D.J.Larson. Atomic scale structure of sputtered metal multilayers[J]. Acta materialia. 49 (2001) 4005～4015.

[12] H.N.G.Wadley, X.Zhou, R.A.Johnson, M.Neurock. Mechanisms, Models and Methods of Vapor deposition. Progress in Materials Science. 46 (2001) 329-377.

[13] D. Farkasa, M. Durandurua, W. A. Curtinb , C. Ribbensc. Multiple-dislocation emission from the crack tip in the ductile fracture of Al 81(2001)1241-1255.

[14] K. Gall, M.F. Hostemeyer, M.V. Schilfgaarde, M.I. Baskes, Atomistic simulations on the tensile debonding of an aluminum–silicon interface. J Mech Phys Solids, 48 (2000) 2183–212.

[15] C.R.Dandekar, Yung C. Shin, Molecular dynamics based cohesive zone law for describing Al-SiC interface mechanics. Composites: Part A 42 (2011) 355–363.

[16] H. Krull, Huang Yuan. Suggestions to the cohesive traction-separation law from atomistic simulations. Engineering Fracture Mechanics. 78 (2011) 525-533.